Nutrient cycling in bedform induced hyporheic zones

Nutrient cycling in bedform induced hyporheic zones.

Revised version

December 23, 2011

L. Bardini[1], F. Boano[1], M. B. Cardenas[2], R. Revelli[1] and L. Ridolfi[1]

[1]Department of Hydraulics, Transports, and Civil Infrastructures, Politecnico di Torino, Corso Duca degli Abruzzi 24, 10129 Turin, Italy.

[2]Department of Geological Sciences, University of Texas at Austin, Austin, Texas 78712, USA.

Abstract

The hyporheic zone is an ecotone connecting the stream and groundwater ecosystem that plays a significant role for stream biogeochemistry. Water exchange across the stream-sediment interface and biochemical reactions in the streambed concur to affect subsurface solute concentrations and eventually nutrient cycling in the fluvial corridor. In this paper we investigate the interplay of hydrological and biochemical processes in a duned streambed and their effect on spatial distribution of solutes. We employ a numerical model to simulate the turbulent water flow and the pressure distribution over the dunes, and then to evaluate the flow field and the biochemical reactions in the hyporheic sediments. Sensitivity analyses are performed to analyze the influence of hydrological and chemical properties of the system on solute reaction rates. The results demonstrate the effect of stream velocity and sediment permeability on the chemical zonation. **Changing sediment permeability as well as stream velocity directly affects the nutrient supply and the residence times in the streambed, thus controlling the reaction rates under the dune.** Stream water quality is also shown to influence the reactive behavior of the sediments. In particular, the availability of dissolved organic carbon determines whether the streambed acts as a net sink or source of nitrate. This study represents **a step towards** a better understanding of the complex interactions between hydrodynamical and biochemical processes in the hyporheic zone.

1 INTRODUCTION

Majority of the world's rivers transports high levels of nutrients, such as organic carbon, nitrate and phosphate, due to anthropogenic activities (Boyer et al., 2006; Mulholland et al., 2008). In the last decades, the fate of these nutrients has attracted the interest of several researchers and, in particular, many studies have shown the significant role played on nutrient cycling by the exchange processes with the hyporheic zone, i.e. the interface region between stream water and groundwater (e.g., Findlay, 1995; Brunke et al., 1997; Boulton et al., 1998; Tonina and Buffington, 2009a).

The hyporheic fluxes occur generally in response to variations in bed topography (Tonina and Buffington, 2009b), with a very wide range of spatial and temporal scales (Cardenas, 2008b; Stonedahl, 2010). Small-scale exchanges are mainly induced by river bed forms, like ripples and dunes (Elliott and Brooks, 1997a,b; Packman et al., 2001; Packman et al., 2004; Boano et al., 2007; Cardenas and Wilson, 2007), while large-scale exchanges depend on larger geomorphological features, like pool-riffle pairs (Tonina and Buffington, 2007), step-pool sequences (Harvey and Bencala, 1993) or meander bends (Boano et al., 2006; Cardenas, 2008a,b; Revelli et al., 2008).

The exchange of water and solutes across the streambed has an effect on the ecology of the fluvial environment since it contributes to the connection of surface and subsurface waters, which have very different chemical characteristics. The exchanged chemicals enter the sediments with the water and they are transformed into oxidized or reduced substances by biogeochemical reactions, mediated by the hyporheic **microbiota**. In particular, organic substances are used as electron donors in a series of redox reactions, with different electron acceptors, e.g., oxygen and nitrate. Nitrification and other secondary reactions often occur as soon as water enters the hyporheic zone (Hunter et al., 1998). These sediment-scale transformations have an influence on the quality of the upwelling water and potentially also on the quality of the stream water. **For example, Böhlke et al. (2009) demonstrated with field measurements that benthic denitrification contributes substantially to nitrate removal in streams.**

The interaction of hydrology and biogeochemistry in the hyporheic zone was taken into

account in different studies of both fluvial **(e.g., Gu et al., 2007; Lautz and Fanelli, 2008; O'Connor and Hondzo, 2008) and marine (e.g. Meysman et al., 2007) environments. In particular, Harvey and Fuller (1998) and Fuller and Harvey (2000) provided observations of solute concentration gradients and reaction rates beneath bedforms in real streams, determining the role of the hyporheic zone in enhancing microbially mediated processes.** Recently, mathematical models have been increasingly used to investigate the effect of coupled hydrological and biogeochemical processes on the fate of nutrients. For instance, Cardenas et al. (2008) provided a model for a rippled permeable seabed, by sequentially modeling turbulent-oscillatory flow, porous media flow, and biogeochemical reactions. Another modeling approach was suggested by Boano et al. (2010), who investigated the biogeochemical patterns and the temporal evolution of reactive solutes in the hyporheic region of a meandering river, by estimating and comparing the typical kinematic and chemical timescales. However, we are still far from a complete understanding of the complex links between hydrodynamical and biogeochemical processes in the hyporheic zone (Fleckenstein et al., 2010).

In this paper, we focus on the influence of surface water-groundwater exchange on the main microbial transformations of nutrients occurring in the hyporheic zone. In particular we develop a numerical model to analyze the exchange triggered by a duned streambed, that represents a widespread configuration in fluvial environments. Our aim is to shed light on the effects of this kind of bed forms on transport and reaction processes of organic carbon and nitrogen, in order to provide significant insights for stream biogeochemistry. The main results of the study are the description of the steady-state spatial distribution of water-borne solutes below a stream dune and the analysis of the effects of stream water quality, stream velocity, and sediment permeability on the reaction patterns. In particular, we take into account four representative reactive compounds: dissolved organic carbon (DOC), oxygen (O_2), nitrate (NO_3^-) and ammonium (NH_4^+). We chose these chemicals because they are usually used as indicators of water quality in field studies (Aitkenhead-Peterson et al., 2009) and they have a direct influence on the equilibrium of the river ecosystem.

The paper is divided in two parts, i.e. the model description, followed by the sensitivity analyses. The simulation of the turbulent water flow represents the preliminary step for the modeling: we numerically solve the Reynolds-Averaged Navier Stokes (RANS) equations in order to obtain the pressure distribution over the dunes. Then, given the RANS-derived surficial pressure gradients, the hyporheic flow field is obtained by applying the Darcy's law. Longitudinal groundwater flow, induced by the stream bed slope, is also considered. The biogeochemical two-dimensional model is finally applied by coupling the chemical reactions with both the hyporheic advective flow field and fluxes induced by hydrodynamic dispersion, under appropriate boundary conditions.

The sensitivity analyses of the biochemical model are carried out for different hydrodynamic and chemical configurations. We study the effect of stream velocity, surface water chemistry, and sediment characteristics on the nutrient dynamics, in order to better understand the links between the hydrodynamic processes and the nutrient transformation rates in the hyporheic zone.

2 MODEL DESCRIPTION

The problem of interest is sketched in Fig. 1. We consider a stream with mean water depth, d, and bulk velocity, U. The streambed is formed of two-dimensional periodic dunes, triangular in shape, with height H and length L. The dunes are asymmetric because of the constant direction of the stream flow, and the position of the crest (L_c) is shifted towards the downstream end of the dune. A Cartesian reference system is adopted, with x and y as the streamwise and upward coordinates, respectively, and the axis origin is placed at the dune trough. Due to the periodicity of the streambed in the streamwise direction, we focus on a single-dune cell of the 2D domain.

The goal is to estimate the spatial distribution of four solutes under the bed forms in steady-state conditions, given the physical and chemical properties of the stream and the hydraulic properties of the sediments. First, turbulent flow in the stream is simulated, and values of pressure on the streambed are evaluated. Then, we numerically simulate

the solute concentrations below the dune surface by considering both the advective and dispersive flows and the biochemical processes. The compounds of interest are DOC, oxygen, nitrate and ammonium. We chose formaldehyde (CH_2O) to represent the DOC substance for its simple chemical structure and because it can be a degradation product of more complicated DOC compounds. Moreover, it is usually selected as the representative DOC compound for numerical simulations or field investigations concerned with the study of chemical patterns in water (e.g., Hunter et al., 1998).

The governing equations and the modeling scheme of the pressure distribution, the hyporheic flow field and the biogeochemical reactions are described below.

2.1 Pressure Distribution

The turbulent water flow over the dunes is simulated by numerically solving, in steady-state conditions, a finite-volume formulation of the Reynolds-averaged Navier-Stokes (RANS) equations for an incompressible, homogeneous fluid (Cardenas and Wilson, 2007)

$$\frac{\partial U_i}{\partial x_i} = 0 \tag{1}$$

$$\rho U_j \frac{\partial U_i}{\partial x_j} = -\frac{\partial P}{\partial x_i} + \frac{\partial}{\partial x_j}\left(2\mu S_{ij} - \rho\overline{u_j' u_i'}\right) \tag{2}$$

where $i, j = 1, 2$ are spatial indexes corresponding to x and y directions ($x_1 = x$, $x_2 = y$), ρ and μ are water density and dynamic viscosity, respectively, t is time, U_i and u_i' are the time-averaged and turbulent velocity components in x_i direction, respectively, and P is time-averaged pressure. $S_{i,j}$ is the strain rate tensor

$$S_{i,j} = \frac{1}{2}\left(\frac{\partial U_i}{\partial x_j} + \frac{\partial U_j}{\partial x_i}\right), \tag{3}$$

while $-\overline{u_j' u_i'} = \tau_{ij}/\rho$ is the mean strain rate related to the Reynolds stresses (τ_{ij}) by

$$-\overline{u_j' u_i'} = \nu_t \left(2S_{ij}\right) - \frac{2}{3}\delta_{ij} k \tag{4}$$

where ν_t is the kinematic eddy viscosity, δ_{ij} is the Kronecker delta, and k is the turbulent kinetic energy.

The evaluation of the turbulent strain rates requires the adoption of a closure scheme to determine the eddy viscosity ν_t. Here, the $k-\omega$ turbulence closure scheme (Wilcox, 1991) is adopted, with the eddy viscosity

$$\nu_t = \frac{k}{\omega}, \tag{5}$$

the specific dissipation ω,

$$\omega = \frac{\epsilon}{\beta^* k} \tag{6}$$

the turbulence dissipation rate ϵ, and the closure coefficient β^*.

Two additional equations for k and ω are required to complete the closure scheme. The steady state transport equations for k and ω are

$$\rho \frac{\partial \left(U_j k\right)}{\partial x_j} = \rho \tau_{ij} \frac{\partial U_i}{\partial x_j} - \beta^* \rho \omega k + \frac{\partial}{\partial x_j}\left[\left(\mu + \mu_t \sigma_k\right) \frac{\partial k}{\partial x_j}\right] \tag{7}$$

$$\rho \frac{\partial \left(U_j \omega\right)}{\partial x_j} = \alpha \frac{\rho \omega}{k} \tau_{ij} \frac{\partial U_i}{\partial x_j} - \beta \rho \omega^2 k + \frac{\partial}{\partial x_j}\left[\left(\mu + \mu_t \sigma_\omega\right) \frac{\partial \omega}{\partial x_j}\right] \tag{8}$$

The standard closure coefficient values are $\alpha = 5/9$, $\beta = 3/40$, $\beta^* = 9/100$, and $\sigma_k = \sigma_\omega = 0.5$ (Cardenas and Wilson, 2007).

The RANS domain is represented by the water column above a single dune (Fig. 1). **A spatially periodic pressure condition is prescribed on the lateral boundaries, with an additional pressure drop ΔP between the left and right domain sides, in order to consider the stream gradient. We assume therefore that the water columns over two subsequent dunes exhibit the same pressure distribution and a constant difference in magnitude, with lower values downstream. The pressure drop is derived from the bed slope i_b and the dune length L by applying the equation $\Delta P = i_b L g \rho$. A symmetry boundary condition (i.e., no fluxes) is set at the top of the RANS domain since water depth is significantly larger than the dune height ($d \ll H$) and the submergence is high. Thus, the**

free surface is not influenced by the presence of bed forms and it is possible to replace it with the symmetry condition. Finally, no-slip wall boundary conditions ($U_j = 0$) are applied at the bottom of the domain. This allows us to solve the problem for turbulent flow neglecting the influence of the subsurface flow in the sediments on the surface flow, which is a standard assumption since subsurface flow rates are usually much smaller than those in the stream. The RANS simulations are solved using a finite-volume approach with a variable number of grid elements (from 16000 to more than 80000) and a denser node spatial distribution near the bottom of the domain. For further details see Cardenas and Wilson (2007).

From the solution of the RANS model, the pressure distribution on the duned streambed is obtained. Fig. 2 shows some streambed pressure distributions on a 1-meter-long dune for different values of the Reynolds number $Re = U \cdot d/\nu$, where ν is the kinematic water viscosity. All pressure profiles have an asymmetrical shape, with a maximum at $x =$ 0.3 m and a marked minimum at the dune cres ($x = 0.9$ m). The figure shows that an increase of the stream velocity leads to higher values of surface pressures. The resulting pressure gradients determine the water exchange with the sediments, as described in the next section.

2.2 Hyporheic Flow Field and Biochemical Reactions

The pressure distribution over the dune is used as a boundary condition in the multicomponent reactive transport model in order to predict the solute fluxes and concentrations in the hyporheic zone, considering both the fluid dynamics and chemical processes. For this purpose, the hyporheic flow modeling represents a key step, since it determines the advective and dispersive transport patterns of the substances in the hyporheic zone.

The advective exchange of water across a duned streambed can be driven by two mechanisms of "pumping" and "turnover": the former is due to the presence of pressure gradients over the bed forms, the latter is linked to the temporary trapping and release of water by moving bed forms (Elliott and Brooks, 1997a). In this paper we assume that the dunes are not moving, since preliminary numerical simulations (not shown) indicated

that water fluxes induced by turnover are negligible for our system.

The water flow under the bed surface in steady-state conditions is estimated using the groundwater flow equations, i.e., the Darcy's law and the continuity equation

$$\mathbf{q} = -\frac{\kappa}{\mu}\left(\nabla P + \rho g \nabla y\right) \tag{9}$$

$$\nabla^2\left(\frac{P}{\rho g} + y\right) = 0, \tag{10}$$

where $\mathbf{q} = (q_x, q_y)$ is the Darcian velocity vector, κ is the permeability of the porous medium (assumed homogeneous), g is the gravitational acceleration, ρ is the water density, and P is the water pressure in the porous medium. **The velocity q includes both the pumping-induced flow and the basic groundwater flow, the latter due to the stream gradient.** The pressure boundary conditions are described later.

As to the biochemical processes, the model considers three reactions, mediated by subsurface microorganisms: **aerobic respiration, denitrification and nitrification (see Table 1). Reactions r_1 and r_2 describe the heterotrophic DOC biodegradation, with the DOC as the electron donor and the oxygen (aerobic respiration) and nitrate (denitrification) as the electron acceptors, respectively. Reaction r_3 represents nitrification, i.e., the biological autotrophic oxidation of ammonium into nitrate, with oxygen as electron acceptor. Aerobic respiration and nitrification start simultaneously, while denitrification only occurs when oxygen concentration falls under a limiting value, i.e. when anaerobic conditions are established.**

For the definition of the reaction kinetics we follow the approach described by Hunter et al. (1998) and, for redox reactions r_1 and r_2, we consider separetely the rate of DOC oxidation and the rate of the i-th reduction half-reaction.

First-order degradation kinetics is assumed for the DOC oxidation rate Γ_{DOC}

$$\Gamma_{DOC} = k_{DOC} \cdot C_{DOC} \tag{11}$$

where k_{DOC} is the DOC decay constant and C_{DOC} is the DOC molar concentration. The linear kinetics in equation (11) is the simplest way to model DOC degradation, but it could be replaced by more complex formulations (e.g., Monod) at the expense of a higher number of parameters.

The rate of reduction $\Gamma_{red,i}$ of the i-th electron acceptor ($i = 1$ for oxygen, $i = 2$ for nitrate) is estimated by

$$\Gamma_{red,i} = \beta_i \cdot \Gamma_{DOC} \cdot f_i \qquad i = 1, 2 \tag{12}$$

where $\boldsymbol{\beta_i}$ represents the ratio between the moles of transferred electrons per mole of oxidized DOC and the moles of electrons per mole of reduced compound in the i-th reaction, and f_i is the fraction of electrons consumed by the i-th reduction half-reaction. Values of β_i are given in Table 1. The f_i parameter is evaluated with a simplified Monod formulation

$$\boldsymbol{f_i = \left(1 - \sum_{n=0}^{i-1} f_n\right) \cdot \alpha_i} \tag{13}$$

with $\boldsymbol{f_0 = 0}$ and

$$\alpha_i = \begin{cases} \frac{C_i}{C_{i,lim}} & \text{if } C_i < C_{i,lim} \\ 1 & \text{if } C_i \geq C_{i,lim} \end{cases}. \tag{14}$$

α_i is a dimensionless parameter that considers the limitation of $\Gamma_{red,i}$ due to the availability of the i-th reaction electron acceptor, while C_i and $C_{i,lim}$ are, respectively, the molar concentration and the molar limiting concentration of the i-th reaction electron acceptor. **When the electron acceptor exceeds the limiting concentration, the reduction rate is independent of C_i, while in the case of lower concentrations $\Gamma_{red,i}$ is linearly proportional to C_i.**

Lastly, a bimolecular expression is used for the nitrification (r_3) rate Γ_{nitr}

$$\Gamma_{nitr} = k_n \cdot C_{NH_4^+} \cdot C_{O_2} \tag{15}$$

where k_n is the second-order nitrification molar rate coefficient, $C_{NH_4^+}$ and C_{O_2} are the

molar concentrations of ammonium and oxygen, respectively. **Since the aim of the present work is to study the reactive behavior of hyporheic sediments in response to stream water quality and velocity and to sediment properties, we neglect the influence of temperature on reaction kinetics.**

From equations (11–14) we define the net production rates of the four compounds of interest, adopting a negative sign for reaction terms decreasing the solute concentration

$$\frac{\mathrm{d}C_{DOC}}{\mathrm{d}t} = -\Gamma_{DOC} \equiv R_{DOC} \tag{16}$$

$$\frac{\mathrm{d}C_{O_2}}{\mathrm{d}t} = -\Gamma_{red,1} - 2\Gamma_{nitr} \equiv R_{O_2} \tag{17}$$

$$\frac{\mathrm{d}C_{NO_3^-}}{\mathrm{d}t} = -\Gamma_{red,2} + \Gamma_{nitr} \equiv R_{NO_3^-} \tag{18}$$

$$\frac{\mathrm{d}C_{NH_4^+}}{\mathrm{d}t} = -\Gamma_{nitr} \equiv R_{NH_4^+} \tag{19}$$

DOC and ammonium show a negative one-term equation (eqns. (16) and (19)), since they take part as reactants in one process, DOC oxidation half-reaction and nitrification, respectively. Instead, oxygen and nitrate display double-term expressions (eqns. (17) and (18)), with different signs because they act, with different roles, in two reactions. The oxygen is consumed by both aerobic respiration r_1 and nitrification r_3, while nitrate is removed by denitrification r_2 and **produced** by nitrification r_3. The contribution of the different terms varies in time, according to the reactant concentrations.

The overall reaction rates (eqns. (16–19)) are then coupled with the hyporheic flow field (obtained by equations (9) and (10)) and hydrodynamic dispersion in order to define the governing equations of the steady-state reactive solute transport model

$$\theta R_s = \nabla(-\theta \mathbf{D} \nabla C_s + \mathbf{q} \cdot C_s) \qquad s = \mathrm{DOC}, \mathrm{O_2}, \mathrm{NO_3^-}, \mathrm{NH_4^+} \tag{20}$$

where θ **is the sediment porosity**, R_s is the consumption/**production** rate of the com-

pound s, $\mathbf{D}$ is the hydrodynamic dispersion tensor and C_s is the molar concentration of the chemical s. The expressions (20) are valid in steady-state conditions and under the assumptions of no sorption phenomena and no solute source in the porous medium. Dispersion represents a solute transport process, additional to the advective one, contributing to the spreading of the chemicals in the hyporheic zone. In particular, hydrodynamic dispersion combines mechanical dispersion, induced by the local velocity variations, and molecular diffusion, caused by concentration gradients at microscopic level. The elements of the dispersion tensor are (Bear and Verruijt, 1998)

$$\theta D_{ij} = (\alpha_L - \alpha_T) \cdot \frac{q_i q_j}{|\mathbf{q}|} + \delta_{ij} \cdot (\alpha_T |\mathbf{q}| + \theta \cdot \tau D_{mol}) \tag{21}$$

where $i, j = 1, 2$, α_L and α_T are the longitudinal and transversal dispersivities, respectively, τ is the tortuosity factor, and D_{mol} is the molecular diffusion coefficient. The values of the dispersivities α_L and α_T depend on sediment size and heterogeneity of the porous medium.

The biogeochemical model domain is a single dune, triangular in shape (see Fig. 2). As to the boundary conditions, we impose on the lateral boundaries the periodic conditions

$$P(x_{min}, y) = P(x_{max}, y) + \Delta P \tag{22}$$

$$C_s(x_{min}, y) = C_s(x_{max}, y) \tag{23}$$

with x_{min} and x_{max} as the horizontal coordinates of the initial and terminal points of the dune and ΔP as the pressure drop between the lateral boundaries of the domain, **equal to that one applied to the free surface.**

On the upper layer, i.e., on the sediment-water interface, we prescribe a Dirichlet condition with the RANS-derived pressure distribution and the constant solute concentrations in the stream. Finally, a no flow condition is applied to all the chemicals at the bottom of the dune, and the porous media is chosen deep enough so as not to affect the pathlines in the main zone of study, close to the bed surface.

3 RESULTS

The chemical zonation in the streambed is investigated through the numerical simulation of the governing equations of the reactive solute transport model. For this purpose, we employ a numerical code that uses a finite-volume approach, with adaptive meshing and error control. In particular, we choose a non uniform mesh, with a higher node density in the zone of interest, near the bed surface, for a total number of 3781 grid nodes and 7216 triangular elements.

We consider a typical dune triangular geometry, with a length $L = 1$ m, a bed form height $H = 0.075$ m and the crest located at $L_c = 0.9$ m (asymmetric dune, see Fig. 1). The streambed is homogeneous and isotropic, with a porosity $\theta = 0.4$ and a tortuosity factor $\tau = 0.74$, while the mean water depth, d, is 0.5 m. With regard to the reaction constants, we choose values within the ranges suggested by Van Cappellen and Wang (1996). In order to consider a typical average condition, for the nitrification rate constant we use the value $k_n = 5 \cdot 10^{-6}$ L/(mg s), while for the DOC reaction rate we select $k_{DOC} = 5 \cdot 10^{-6}$ s^{-1}. Oxygen and nitrate limiting concentrations ($C_{O_2,lim}$ and $C_{NO_3^-,lim}$) are set at 1 mg/L and 0.5 mg/L, respectively. As to the other physical and chemical parameters, i.e., the in-stream solute concentrations, the stream velocity U, the sediment permeability κ and dispersivities α_L and α_T, we perform a sensitivity analysis in order to investigate their impact on the biochemical processes in the streambed.

3.1 Impact of Stream Water Quality

Three configurations, characterized by different values of in-stream solute concentrations (see Table 2), are considered: a polluted stream, with high nutrient concentrations (case 1), a pristine stream with no DOC limitation (case 2) and a pristine stream with DOC limitation (case 3). **The pristine stream configuration is split in two cases in order to consider the remarkable effects of DOC availability on the kinetics of reactions.** The permeability κ is set equal to 10^{-10} m^2, characteristic of well-sorted coarse sands to gravels. The longitudinal dispersivity is assumed equal to 3 mm (i.e., a few grain diameters), while the transversal dispersivity α_T is a tenth of the longitudinal

one α_L. The stream velocity U is 0.34 m/s and the stream slope is $1.5 \cdot 10^{-4}$.

The results of the simulations are displayed in Fig. 3 (case 1), 4 (case 2) and 5 (case 3). Two advective flow cells are visible below the streambed surface, with different width and depth. The cell in the right-hand part of the dune is wide and quite deep (65 cm); mean flow direction in the cell is the same as the stream flow. On the contrary, the left cell is narrower and shallower, with mean flow opposite to the stream flow. A stagnation point is also present at the deepest point of this cell. Both advective cells delimit an advective water exchange area, where water from the stream moves along advective flowpaths before leaving the sediments, with different residence times depending on path length. Beneath this zone the flow field is dominated by groundwater underflow, induced by the stream slope, and water flow is not affected by the presence of the dunes. **The same reversed hyporheic circulation cells and flow stagnation zones were recently observed in a flume and modeled by CFD from Endreny et al. (2011). The flow cells have a direct influence on solute spatial distribution. In fact, even though dispersion tends to smooth concentration gradients, the solute concentration fronts clearly reflect the shape of the water exchange area.**

The substantial role played by advection and dispersion fluxes is demonstrated in Fig. 6, where oxygen concentrations of case 2 are shown for different dune vertical sections, in the case of diffusive transport only, i.e., switching off water flow and the resulting advective and dispersive fluxes. Oxygen penetration in the porous medium occurs with such a low velocity that the compound is completely removed within the first 5 millimeters of sediments in all the considered sections. Another key point is that the diffusive transport is downward directed, so all solutes entering the sediments are slowly moved to deeper layers and are not returned back to the stream. Thus, the advective and dispersive fluxes are fundamental for controlling the nutrient fate in the streambeds.

We now analyze the three basic cases to investigate the effect of stream water quality. We consider at first the polluted stream configuration shown in Fig. 3.

DOC exhibits a smooth spatial distribution, with two roughly circular fronts of different sizes and concentrations decreasing with depth. In fact, both advection and dispersion are important mechanisms for delivery of DOC into the porous medium, **where it is progressively degraded (eqn. (16)).** Thus, the hyporheic zone acts as a sink of DOC for the stream. However, the DOC is still present at the bottom of the dune with a concentration of 30 mg/L, since it is not a limiting reactant for the two reactions.

Oxygen displays a similar behavior, with concentration decreasing with depth. However, oxygen fronts are steeper than DOC ones, because of the fast oxygen consumption by two contemporary reactions , i.e., **aerobic respiration and nitrification (eqn. (17))**. Moreover, due to the low in-stream oxygen concentration and the high availability of DOC and NH_4^+, oxygen is completely removed within the first 30 cm of depth, i.e. within the water exchange area. **These simulated oxygen distributions reproduce well the general features of the patterns observed experimentally by Precht et al. (2004).**

Ammonium also exhibits steep fronts and remarkable variations of concentration in the hyporheic zone, because of the fast kinetics of the nitrification process in which it plays the part of the reactant (eqn. (19)). Eventually, a concentration of 4.5 mg/L is achieved when **nitrification** stops due to the lack of oxygen. Thus, ammonium spatial distribution is strictly related to the oxygen zonation.

A different behavior is shown by nitrate, which exhibits a maximum concentration at 15 cm of depth (see Fig. 3). The reason for this behavior is that the compound has the double role of product and reactant in the nitrification and denitrification reactions, respectively (eqn. (18)). The removal of nitrate through denitrification begins only when the oxygen falls below the limiting concentration $C_{O_2,lim}$, so up to that threshold the compound is only **produced** by nitrification. **In deeper sediments, denitrification prevails and nitrate is completely removed within the first 35 cm of depth. This behavior is confirmed by Fig. 7a and 7b, that show the spatial patterns of nitrification and denitrification rates. Nitrification rate has a maximum value (0.34** $\mathrm{mg}/(\mathrm{m}^3 \cdot \mathrm{s})$**) near the streambed, due to the high concentrations**

of oxygen and ammonium, and it decreases with depth, as the consequence of the lower reactant concentrations. Instead, denitrification rate displays a downward increase, together with the nitrate concentrations, a maximum value (0.38 $\mathrm{mg}/(\mathrm{m}^3 \cdot \mathrm{s})$**) at approximately 35 cm of depth and a fast decrease. Both reactions are active in the central part of the domain, with different rates; as long as nitrification prevails on denitrification there is a net nitrate production and viceversa. The strong nitrate production within the first 20 cm of depth contributes to enhance the nitrate concentration gradient and, consequently, the upward dispersive fluxes (see equation (20)), that are comparable or higher than the advective ones, with the exception of the dune crest (see Fig. 7c, 7d, 7e, 7f). Part of produced nitrate is released into the stream due to the combination of strong upward advective and dispersive transport, and the dune thus represents a source of nitrate for the stream.**

We focus now on the pristine stream configuration with no DOC limitation (case 2, Fig. 4). All solute in-stream concentrations are lower than in the polluted case, with the exception of oxygen, which keeps the same value (Table 2). The decrease of the solute concentrations has a direct influence on the rate of the three studied reactions. Oxygen shows a more gradual decay and wider concentration fronts, due to the decrease of both aerobic respiration and nitrification rates caused by lower concentrations of DOC and ammonium, respectively. The slower oxygen consumption **leads in turn to a downward shift of the net denitrifying zone. Thus, nitrate and oxygen are completely removed deeper in the porous medium than in case 1. The spatial patterns of nitrification and denitrification rates are shown in Fig. 8a and 8b. The values are in general one or two orders of magnitude lower than those seen for case 1. Besides, the maximum nitrification rate is highly lower than the denitrification one. The lower nitrate production has a direct effect on the magnitude of the dispersive transport of nitrate. Fig. 8c, 8d, 8e and 8f show the advective and dispersive fluxes with the former prevalent on the latter in the shallow layers. In this case the dune represents a sink of nitrate for the stream.**

The wider concentration fronts are even more evident for the pristine stream configuration with DOC limitation (case 3, Fig. 5). **Aerobic respiration** rate is so slow, due to the DOC scarcity, that oxygen can be found even at the bottom of the streambed (6 mg/L), preventing the denitrification process which requires anaerobic conditions. **Thus, denitrification does not occur in the sediments in this case. Aerobic respiration is active up to the bottom of the streambed, while nitrification stops shallower, at 60 cm of depth, for lack of ammonium. For this reason nitrate concentrations show an increase with depth up to 60 cm of depth, while they keep a constant value under that layer. As seen for case 1, the hyporheic zone behaves as a net nitrate source because of the strong nitrate dispersive transport (induced by nitrate production), upward directed, near the bed surface.**

The different behavior of the hyporheic zone in the three cases is clearly underlined by the values of the Integrated oxygen Aerobic Respiration rates (IAR) and **the Nitrification** (IN) and Denitrification (ID) rates (see Table 3)

$$IAR = \int_{A_s} \Gamma_{red,1} \cdot \mathrm{d}A, \tag{24}$$

$$IN = \int_{A_s} \Gamma_{nitr} \cdot \mathrm{d}A, \tag{25}$$

$$ID = \int_{A_s} \Gamma_{red,2} \cdot \mathrm{d}A, \tag{26}$$

where A_s is the subsurface domain area, i.e. the volume of sediments per unit stream width.

Table 3 shows that aerobic respiration rate IAR increases with increasing in-stream concentrations of DOC **(e.g., compare cases 2 and 3). In fact, increasing in-stream DOC concentration concurs to increase oxygen reduction rate $\Gamma_{red,1}$ (see equations (11) and (12)), and thus IAR.**

If we focus on nitrate, the ratio between ID and IN indicates the reactive behavior of the dune as a net sink (ID/IN $>$ 1) or source (ID/IN $<$ 1) of nitrate. This happens because there is no net solute flux trough the lateral

boundaries due to the periodic boundary conditions, and thus net nitrate production equals net exchange flux through the streambed. In Table 3 we observe that the hyporheic zone can act as a net source of nitrate in both polluted and pristine streams (cases 1 and 3), despite these cases representing two seemingly opposite chemical conditions. The DOC availability is a discriminating parameter for the degradation rates in pristine streams**; high concentrations of labile DOC enhance both aerobic respiration and denitrification rates, leading to a faster removal of oxygen and a net consumption of nitrate in hyporheic sediments.**

3.2 Impact of Stream Velocity

Increasing stream velocity values are considered for the three cases in Table 2, in order to estimate and compare the solute reaction rates, reflecting the behavior of the streambed. The stream velocity ranges from 0.21 m/s to 0.39 m/s, which correspond to Reynolds number Re between 106670 and 195630.

A variation of the stream velocity induces two opposite effects on solute reactions. From a hydrodynamical point of view, an increase in U implies higher inward water fluxes due to the higher pressure gradients on the dune surface. This leads to larger fluxes of substances from the stream to the sediments which can enhance reaction rates. Neverthless, hyporheic microbes have less time for performing biochemical reactions because of the lower residence time of the compounds in the streambed, potentially leading to lower reaction rates. The net effect on reaction rates depends on the interaction between these opposite factors, i.e, higher solute inputs and lower residence times (Arnon et al., 2007; Cardenas et al., 2008).

Looking at the results (Table 4), it can be observed that all integrated solute reaction rates increase with the stream velocity, even if with different relative variations. In particular, the IN parameter shows a higher sensitivity to the stream velocity variations than the other ones, with consequences on the general streambed reactive behavior. These trends demonstrate **that in the simulated conditions the increase of inward solute fluxes, with U, have a predominant role for the solute reaction rate, while the decrease of the residence times in the porous medium is less important.**

As to the net nitrate production rate, we consider the ratio of ID to IN. Fig. 9 shows that the increase of the stream velocity does not change dramatically the streambed behavior but it clearly leads to limiting the sink role (case 2), and to enhance the source role (case 1) of the hyporheic zone. This behavior is the result of **a higher sensitivity of nitrification to stream velocity, compared to denitrification.**

3.3 Impact of Sediment Hydraulic and Transport Properties

We focus on the pristine stream configuration with no DOC limitation (case 2). **Although recently it has been demonstrated that sediment permeability heterogeneity influences hyporheic exchange (Sawyer and Cardenas, 2009), in this section the role of permeability is investigated, under the hypothesis of homogeneity, for the sake of simplicity.** The stream velocity U is set to the constant value of 0.27 m/s, while the sediment permeabilities and dispersivities are varied to investigate the influence of the size of sediment grains **(see Table 5).** Since dispersivity is proportional to the sediment grain size, d_g, and permeability **scales** with d_g^2, it follows that a ten-fold increase in κ results in approximately a three-fold increase in α_L. Again, values of the transversal dispersivities α_T are chosen as a tenth of the longitudinal ones.

The results underline a marked effect of the permeability on the solute spatial distribution (see Fig. 10), with less steep fronts corresponding to higher values of permeability and dispersivity. The increase of κ, α_L and α_T results in more efficient advective and dispersive transport and enhanced solute penetration. For $\kappa = 10^{-11}$ m^2 DOC degradation is fast and the compound is completely removed within the first 30 cm of depth (Fig. 10a), while for $\kappa = 5 \cdot 10^{-10}$ m^2 high DOC values (38 mg/L) are still present at the bottom of the streambed (Fig. 10d). It is also interesting to observe the different streambed aerobic conditions in the opposite cases, with the aerobic zone confined in the shallower layers for the low permeability case and filling almost all the porous medium for the high permeability case.

The integrated reaction rates show an increase with increasing sediment permeability (Table 5), with different sensitivities. This behavior is caused by the higher nutrient supply

from the stream with increasing permeability, and is similar to the effect of increasing stream velocity. Values of IN show that nitrification, more than denitrification, is sensitive to permeability, which leads to a shift from the hyporheic zone acting as a net nitrate sink (ID/IN > 1) to source (ID/IN < 1) with increasing κ.

4 CONCLUSIONS

The solute spatial distribution in the hyporheic zone is due to a strong interplay of both hydraulic and biogeochemical processes. Nutrients enter the sediments because of pressure-induced water exchanges, and there they are both transported by advective and dispersive fluxes, and then biochemically transformed by hyporheic **microbiota**. So, a variation of the transport conditions or the chemical kinetics, induced by different stream and sediment characteristics, can have a direct influence on the reaction potential of the streambed, **with ecological implications. If we focus on the hyporheic fauna, the exchanges of water, nutrients and organic matter through the streambed and the chemical concentrations in the sediments are fundamental for microbiota and invertebrates.**

Our simulations show that the stream water quality can strongly affect the biochemical reactions. In general, the streambed always acts as a sink of DOC, oxygen and ammonium, while nitrate, that is subject to production and consumption reactions, displays a more complex behavior. In the considered cases, high in-stream concentrations of solutes have been shown to enhance **nitrification** process leading to strong nitrate production in the porous medium. In these conditions the hyporheic zone behaves as a nitrate source for the stream. In pristine streams nitrate fate has proved to be strictly linked to DOC availability. A scarcity of DOC can limit denitrification and prevent nitrate removal, leading to a streambed acting as a nitrate source. Instead, high concentrations of DOC favour denitrification and lead to a net nitrate consumption.

Stream velocity and sediment permeability have displayed a direct effect on transport phenomena. Increasing stream velocity implies larger solute fluxes to sediments but also lower residence times of the compounds in the hyporheic zone and a lower time for reac-

tions. In our simulations, the higher solute supply clearly prevails over the lower residence times, since all reaction rates increase with stream velocity. In particular, nitrification appears to be more sensitive to changes in stream velocity than denitrification. The consequence is that high stream velocities damp the sink role and enhance the source role of the streambed. The hydraulic properties of sediments have a similar influence on solute spatial distribution. Higher values of permeability improve the transport efficiency and increase reaction rates, strongly affecting the reactive behavior of the hyporheic zone. In particular, high-permeability sediments enhance nitrate production and can induce a switch from nitrate sink to source behavior.

Acknowledgments F.B. and R.R. would like to thank the Italian Ministry of University and Research (MIUR) for supporting the research with PRIN 2008A7EBA3_002 "Role of interactions between surface water and groundwater in the transport of solutes at slope scale". L.B. also thanks the MIUR for funding the PhD project. M.B.C. was supported by a National Science Foundation CAREER grant (EAR-0955750).

References

[Aitkenhead-Peterson J. A., Steele M. K., Nahar N. and Santhy K. (2009)] Dissolved organic carbon and nitrogen in urban and rural watersheds of south-central Texas: land use and land management influences, *Biogeochemistry* **96**, pp. 119–129, doi:10.1007/s10533-009-9348-2.

[Arnon et al. (2007)] Arnon S., Gray K. A. and Packman A. I. (2007a) Biophysicochemical process coupling controls nitrate use by benthic biofilms, *Limnol. Oceanogr.* **52**(4), pp. 1665–1671.

[Bear and Verruijt, 1998] Bear J. and Verruijt A. (1998) *Modeling groundwater flow and pollution*, D. Reidel Publishing Company, Dordrecht, Holland

[Boano et al., 2006] Boano F., Camporeale C., Revelli R. and Ridolfi L. (2006) Sinuosity-driven hyporheic exchange in meandering rivers, *Geophys. Res. Lett.* **33**, L18406, doi:10.1029/2006GL027630.

[Boano et al., 2007b] Boano F., Revelli R. and Ridolfi L. (2007b) Bedform-induced hyporheic exchange with unsteady flows, *Adv. Water Resour.* **30**(1), pp. 148–156.

[Boano et al., 2010] Boano F., Demaria A., Revelli R. and Ridolfi L. (2010) Biogeochemical zonation due to intra–meander hyporheic flow, *Water Resour. Res.* **46**, W02511, doi:10.1029/2008WR007583.

[Bottacin-Busolin and Marion, 2010] Bottacin-Busolin A. and Marion A. (2010) Combined role of advective pumping and mechanical dispersion on time scales of bed forms-induced hyporheic exchange, *Water Resour. Res.* **46**, W08518, doi:10.1029/2009WR008892.

[Boulton et al., 1998] Boulton A. J., Findlay S., Marmonier P., Stanley E. H. and Valett H. M. (1998) The functional significance of the hyporheic zone in streams and rivers, *Annu. Rev. Ecol. Syst.* **29**, pp. 59–81.

[Boyer et al., 2006] Boyer E. W., Howarth R. W., Galloway J. N. et al. (2006) Riverine nitrogen export from the continents to the coasts, *Glob. Biogeochem. Cycle* **20**(1), GB1S91.

[Brunke and Gonser, 1997] Brunke M. and Gonser T. (1997) The ecological significance of exchange processes between rivers and groundwater, *Freswater Biol.* **37**, pp. 1–33, doi:10.1046/j.1365-2427.1997.00143.x.

[Cardenas, 2008a] Cardenas M. B. (2008a) The effect of river bend morphology on flow and timescales of surface water-groundwater exchange across pointbars, *J. Hydrol.* **362**(1–2), pp. 134–141.

[Cardenas, 2008b] Cardenas M. B. (2008b) Surface water-groudwater interface geomorphology leads to scaling of residence times, *Geophys. Res. Lett.* **35**, L08402, doi:10.129/2008GL033753.

[Cardenas and Wilson, 2007] Cardenas M. B. and Wilson J. L. (2007) Dunes, turbulent eddies, and interfacial exchange with permeable sediments, *Water Resour. Res.* **43**, W08412, doi: 10.1029/2006WR005787.

[Cardenas et al., 2008] Cardenas M. B., Cook P., Jiang and Traykovski H. (2008) Constraining denitrification in permeable wave-influenced marine sediment using linked hydrodinamic and biogeochemical modeling, *Earth Planet. Sci. Lett.* **275**, pp. 127–137.

[Elliott and Brooks, 1997a] Elliott A. H. and Brooks N. H. (1997a) Transfer of nonsorbing solutes to a streambed with bed forms: Theory, *Water Resour. Res.* **33**(1), pp. 123–136.

[Elliott and Brooks, 1997b] Elliott A. H. and Brooks N. H. (1997b) Transfer of nonsorbing solutes to a streambed with bed forms: Laboratory experiments, *Water Resour. Res.* **33**(1), pp. 137–151.

[Findlay, 1995] Findlay S. (1995) Importance of surface-subsurface exchange in stream ecosystems: The hyporheic zone, *Limnol. Oceanogr.* **40**, pp. 159–164.

[Fleckenstein et al., 2010] Fleckentein J. H., Krause S., Hannah D. M. and Boano F. (2010) Groundwater-surface water interactions: new methods and models to improve understanding of processes and dynamics, *Adv. Water Resour.* **33**(11), pp. 1291–1295.

[Gu et al., 2007] Gu C., Hornberger G. M., Mills A. L., Herman J. S. and Flewelling S. A. (2007) Nitrate reduction in streambed sediments: Effects of flow and biogeochemical kinetics, *Water Resour. Res.* **43**, W12413, doi:10.1029/2007WR006027.

[Harvey and Bencala, 1993] Harvey J. W. and Bencala K. E. (1993) The Effect of Streambed Topography on Surface-Subsurface Water Exchange in Mountain Catchments, *Water Resour. Res.* **29**(1), pp. 8998, doi:10.1029/92WR01960.

[Hunter and Van Cappellen, 1998] Hunter K. S., Wang Y. and Van Cappellen P. (1998) Kinetic modeling of microbially-driven redox chemistry of subsurface environments: Coupling transport, microbial metabolism and geochemistry, *J. Hydrol.* **209**, pp. 53–80.

[Lautz and Fanelli, 2008] Lautz L. K. and Fanelli R. M. (2008), Seasonal biogeochemical hotspots in the streambed around restoration structures, *Biogeochemistry* **91**, pp. 85–104.

[Meysman et al., 2007] Meysman F.J.R., Galaktionov O. S., Cook P. L. M., Janssen F., Huettel M. and Middelburg J. J. (2007) Quantifying biologically and physically induced flow and tracer dynamics in permeable sediment, *Biogeosciences* **4**, pp. 627–646.

[Mulholland et al., 2008] Mulholland P. J., Helton A. M., Poole G. C. et al. (2008) Stream denitrification across biomes and its response to anthropogenic nitrate loading, *Nature* **452**(7184), pp. 202–246.

[Packman and Brooks, 2001] Packman A. I. and Brooks N. H. (2001) Hyporheic exchange of solutes and colloids with moving bed forms, *Water Resour. Res.* **37**(10), pp. 2591–2605.

583 [Packman et al., 2004] Packman A. I., Salehin M. and Zaramella M. (2004) Hyporheic
584 exchange with gravel beds: basic hydrodinamic interactions and bedform-induced ad-
585 vective flows, *J. Hydraul. Eng.* **130**, pp. 647–656.

586 [Revelli et al., 2008] Revelli R., Boano F., Camporeale C. and Ridolfi L. (2008) In-
587 trameander hyporheic flow in alluvial rivers, *Water Resour. Res.* **44**, W12428,
588 doi:10.1029/2008WR007081.

589 [Stonedahl et al., 2010] Stonedahl S. H., Harvey J. W., Wrman A., Salehin M. and Pack-
590 man A. I. (2010) A multiscale model for integrating hyporheic exchange from ripples to
591 meanders, *Water Resour. Res.* **46**, W12539, doi:10.1029/2009WR008865.

592 [Tonina and Buffington, 2007] Tonina D. and Buffington J. M. (2007) Hyporheic exchange
593 in gravel bed rivers with pool-riffle morphology: Laboratory experiments and three-
594 dimensional modeling, *Water resour. Res.* **43**, W01421, doi:10.1029/2005WR004328.

595 [Tonina and Buffington, 2009a] Tonina D. and Buffington J. M. (2009a) Hyporheic Ex-
596 change in Mountain Rivers I: Mechanics and Environmental Effects, *Geography Compass*
597 **3**, doi: 10.1111/j.1749-8198.2009.00226.x.

598 [Tonina and Buffington, 2009b] Tonina D. and Buffington J. M. (2009b) Hyporheic Ex-
599 change in Mountain Rivers II: Effects of Channel Morphology on Mechanics, Scales,
600 and Rates of Exchange, *Geography Compass* **3**, doi: 10.1111/j.1749-8198.2009.00225.x.

601 [Van Cappellen and Wang, 1996] Van Cappellen P. and Wang Y. (1996) Cycling of iron
602 and manganese in surface sediments: a general theory for the coupled transport and
603 reaction of carbon, oxygen, nitrogen, sulfur, iron and manganese, *Am. J. Sci.* **296**, pp.
604 197-243.

605 [Packman and Brooks, 2001] Packman A. I. and Brooks N. H. (2001) Hyporheic exchange
606 of solutes and colloids with moving bed forms, *Water Resour. Res.* **37**(10), pp. 2591–
607 2605.

608 [Packman et al., 2004] Packman A. I., Salehin M. and Zaramella M. (2004) Hyporheic
609 exchange with gravel beds: basic hydrodinamic interactions and bedform-induced ad-
610 vective flows, *J. Hydraul. Eng.* **130**, pp. 647–656.

611 [Revelli et al., 2008] Revelli R., Boano F., Camporeale C. and Ridolfi L. (2008) In-
612 trameander hyporheic flow in alluvial rivers, *Water Resour. Res.* **44**, W12428,
613 doi:10.1029/2008WR007081.

614 [Stonedahl et al., 2010] Stonedahl S. H., Harvey J. W., Wrman A., Salehin M. and Pack-
615 man A. I. (2010) A multiscale model for integrating hyporheic exchange from ripples to
616 meanders, *Water Resour. Res.* **46**, W12539, doi:10.1029/2009WR008865.

617 [Tonina and Buffington, 2007] Tonina D. and Buffington J. M. (2007) Hyporheic exchange
618 in gravel bed rivers with pool-riffle morphology: Laboratory experiments and three-
619 dimensional modeling, *Water resour. Res.* **43**, W01421, doi:10.1029/2005WR004328.

620 [Tonina and Buffington, 2009a] Tonina D. and Buffington J. M. (2009a) Hyporheic Ex-
621 change in Mountain Rivers I: Mechanics and Environmental Effects, *Geography Compass*
622 **3**, doi: 10.1111/j.1749-8198.2009.00226.x.

623 [Tonina and Buffington, 2009b] Tonina D. and Buffington J. M. (2009b) Hyporheic Ex-
624 change in Mountain Rivers II: Effects of Channel Morphology on Mechanics, Scales,
625 and Rates of Exchange, *Geography Compass* **3**, doi: 10.1111/j.1749-8198.2009.00225.x.

626 [Van Cappellen and Wang, 1996] Van Cappellen P. and Wang Y. (1996) Cycling of iron
627 and manganese in surface sediments: a general theory for the coupled transport and
628 reaction of carbon, oxygen, nitrogen, sulfur, iron and manganese, *Am. J. Sci.* **296**, pp.
629 197-243.

Table 1: List of the reactions considered in the simulations.

Reaction index	Reaction type	Reaction	β value
r_1	Aerobic respiration	$CH_2O + O_2 \longrightarrow CO_2 + H_2O$	1
r_2	Denitrification	$5CH_2O + 4NO_3^- + 4H^+ \longrightarrow 5CO_2 + 2N_2 + 7H_2O$	0.8
r_3	Nitrification	$NH_4^+ + 2O_2 \rightarrow NO_3^- + 2H^+ + H_2O$	-

Table 2: Solute in-stream concentrations for cases 1, 2 and 3.

Case	$C_{DOC,0}$ mg/L	$C_{O_2,0}$ mg/L	$C_{NO_3^-,0}$ mg/L	$C_{NH_4^+,0}$ mg/L
1	150	10	8	5.00
2	50.0	10	1	0.05
3	5.00	10	1	0.05

Table 3: IAR, ID and IN rates for cases 1, 2 and 3.

Case -	IAR μg/(m·s)	ID μg/(m·s)	IN μg/(m·s)	ID/IN -
1	106	31.4	55.9	0.56
2	49.5	1.14	0.87	1.31
3	6.14	0	1.08	0

Table 4: IAR, ID and IN rates for cases 1, 2 and 3, with different stream velocities.

Case -	U m/s	IAR μg/(m·s)	ID μg/(m·s)	IN μg/(m·s)	ID/IN -
1	0.21	78.1	26.6	38.1	0.7
1	0.24	85.8	28.1	42.8	0.66
1	0.27	93.2	29.4	47.5	0.62
1	0.30	100	30.5	52.0	0.59
1	0.33	106	31.4	55.9	0.56
1	0.36	111	32.2	59.4	0.54
1	0.39	116	32.9	62.8	0.52
2	0.21	38.3	1.05	0.62	1.68
2	0.24	41.4	1.08	0.69	1.57
2	0.27	44.4	1.11	0.76	1.47
2	0.30	47.2	1.13	0.82	1.39
2	0.33	49.5	1.14	0.87	1.31
2	0.36	51.5	1.15	0.92	1.25
2	0.39	53.4	1.15	0.96	1.19
3	0.21	4.99	0	0.80	0
3	0.24	5.32	0	0.88	0
3	0.27	5.63	0	0.95	0
3	0.30	5.91	0	1.02	0
3	0.33	6.14	0	1.08	0
3	0.36	6.33	0	1.13	0
3	0.39	6.50	0	1.18	0

Table 5: IAR, ID and IN rates for case 2, with different permeabilities and dispersivities.

$10^{11} \cdot \kappa$ m^2	α_L mm	α_T mm	IAR μg/(m·s)	ID μg/(m·s)	IN μg/(m·s)	ID/IN -
1.00	1.00	0.10	13.2	0.54	0.18	3.09
5.00	2.20	0.22	33.1	0.97	0.52	1.88
10.0	3.00	0.30	44.4	1.11	0.76	1.47
50.0	6.60	0.66	76.9	1.49	1.58	0.94

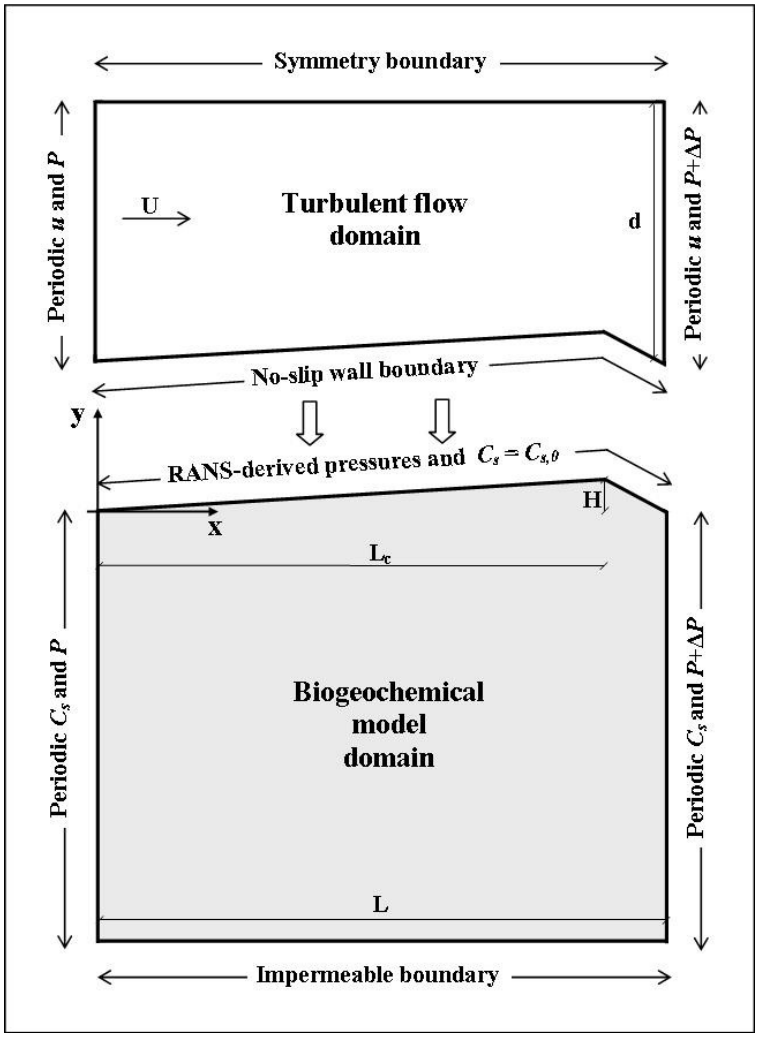

Fig. 1. Modeling scheme. Top part shows the pressure and velocity boundary conditions for the stream water turbulent flow over the streambed; bottom part shows the pressure and concentration boundary conditions for the solute reactive transport in the porous medium. The model domain represents an asymmetrical stream dune of length L = 1 m, height H = 0.075 m, with the crest shifted on the right (L_c = 0.9 m). The streambed depth is 0.8 m. The stream velocity U varies from 0.21 to 0.39 m/s in the simulations.

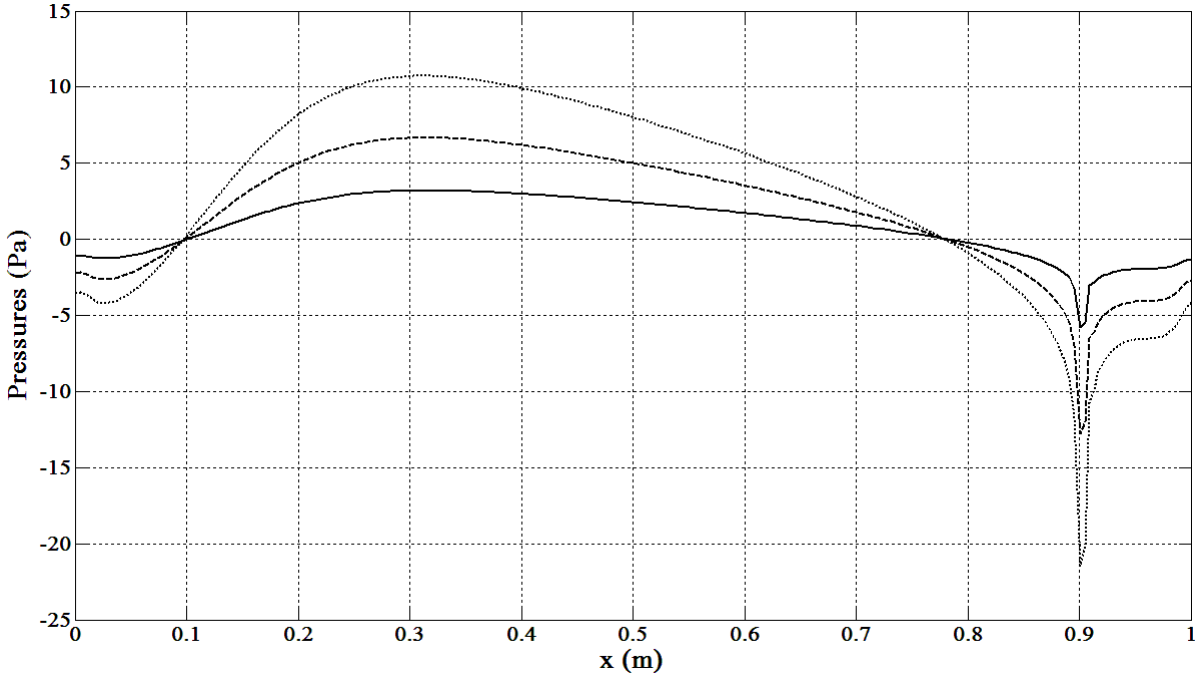

Fig. 2. RANS-derived pressure distributions for stream velocities U = 0.21 m/s (solid line), 0.30 m/s (dashed line) and 0.39 m/s (dotted line), corresponding to Reynolds numbers Re = 106670, 154120 and 195630, respectively (L = 1 m, L_c = 0.9 m, H = 0.075 m, d = 0.5 m).

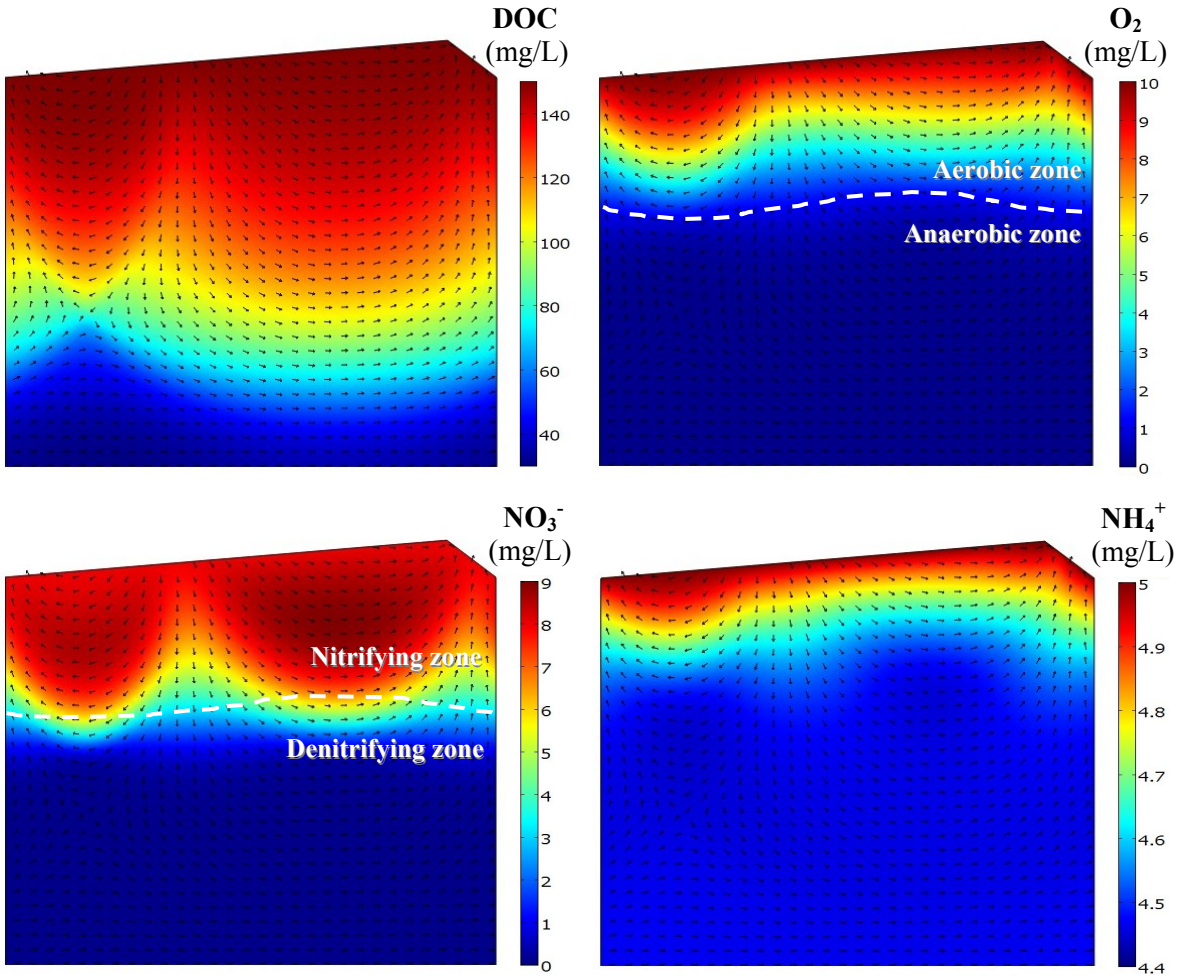

Fig. 3. Solute spatial distribution for the polluted stream (case 1). Stream velocity is U = 0.33 m/s, sediment permeability is $\kappa = 10^{-10}$ m^2, longitudinal dispersivity is α_L = 3 mm. DOC reaction rate is $k_{DOC} = 5 \cdot 10^{-6}$ s^{-1}, nitrification rate is $k_n = 5 \cdot 10^{-6}$ L/(**mg**·**s**). In-stream concentrations are shown in Table 2. Vectors are only indicative of flow direction.

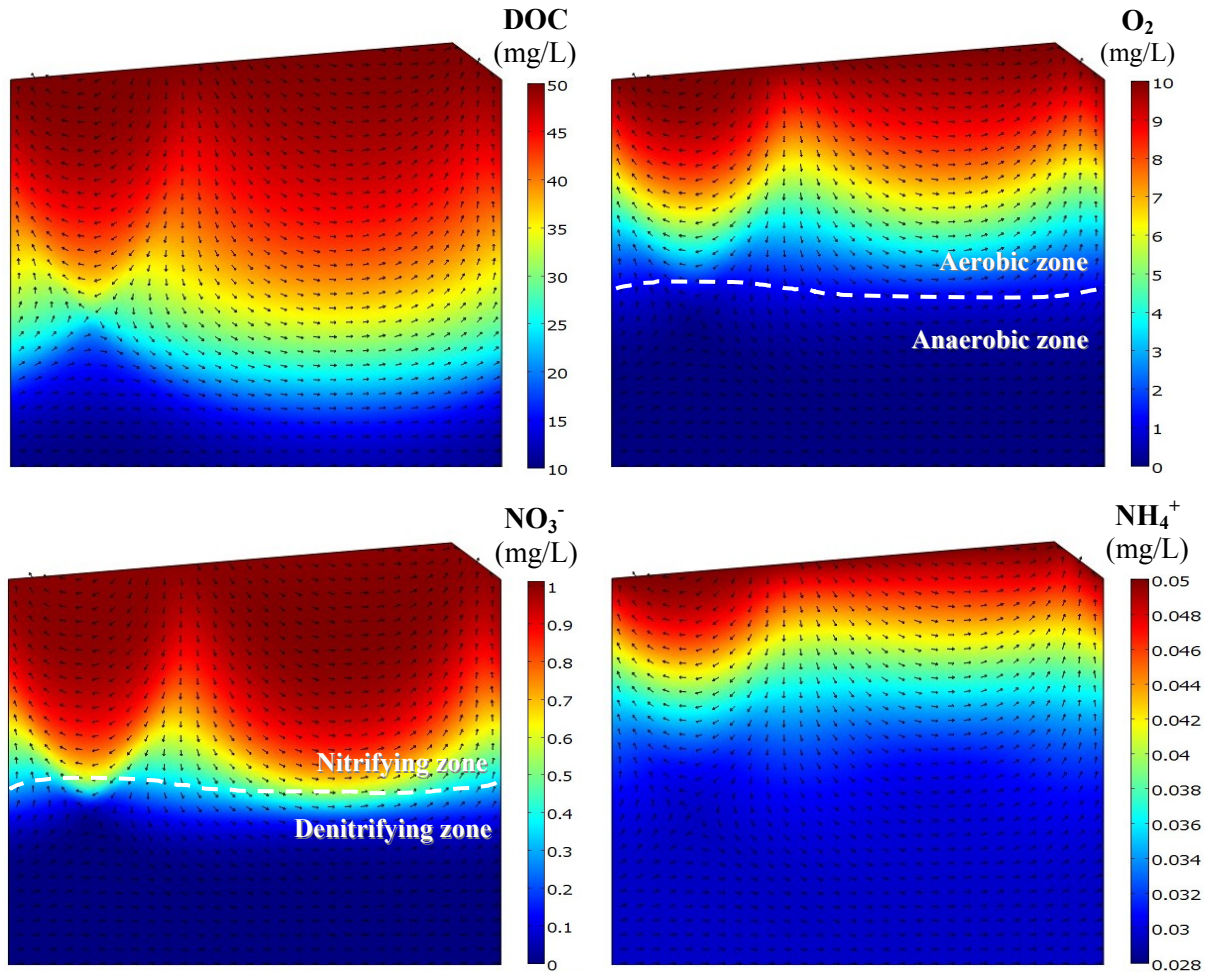

Fig. 4. Solute spatial distribution for the pristine stream with no DOC limitation (case 2). Stream velocity is U = 0.33 m/s, sediment permeability is $\kappa = 10^{-10}$ m^2 and longitudinal dispersivity is α_L = 3 mm. DOC reaction rate is $k_{DOC} = 5 \cdot 10^{-6}$ s^{-1}, nitrification rate is $k_n = 5 \cdot 10^{-6}$ L/(**mg**·**s**). In-stream concentrations are shown in Table 2. Vectors are indicative of flow direction.

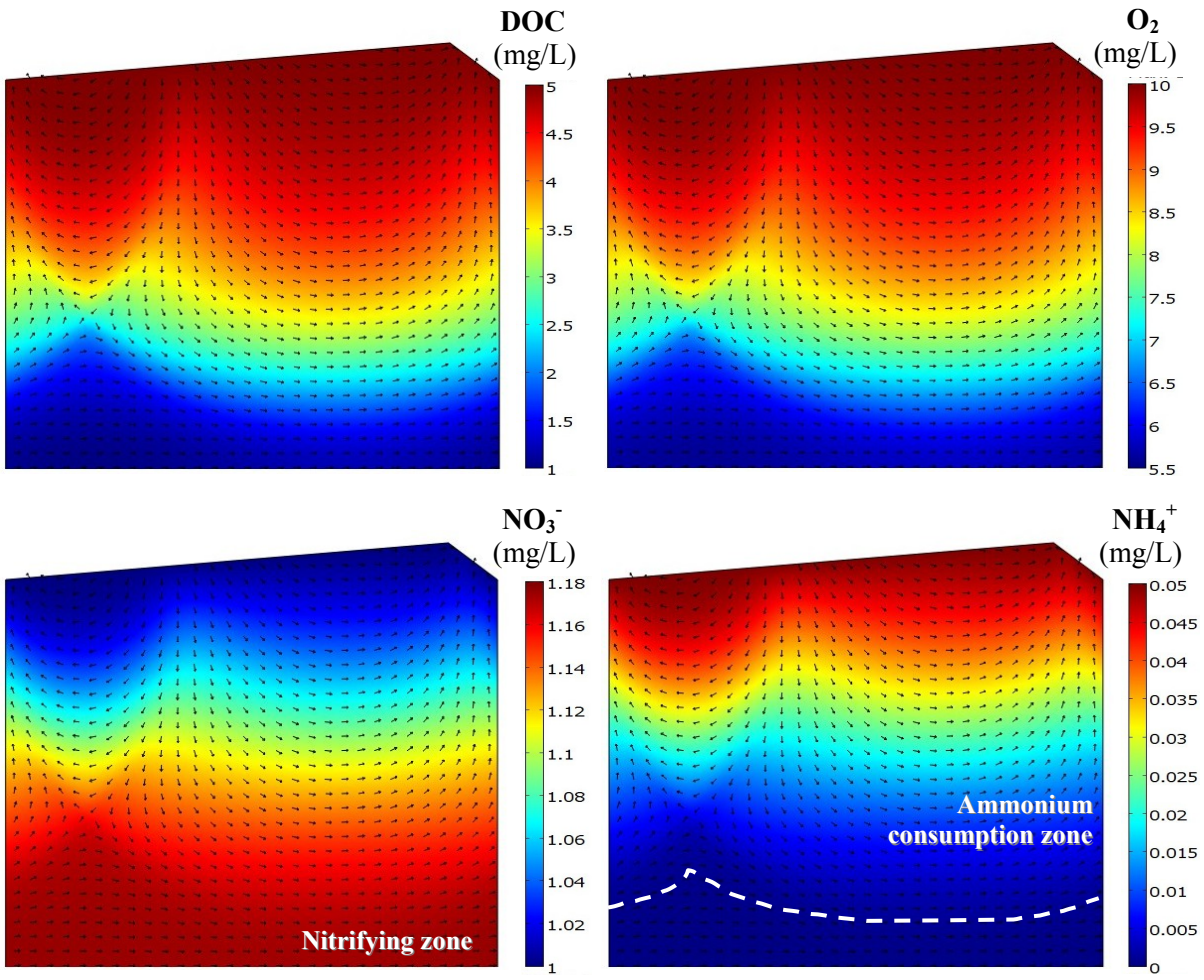

Fig. 5. Solute spatial distribution for the pristine stream with DOC limitation (case 3). Stream velocity is U = 0.33 m/s, sediment permeability is $\kappa = 10^{-10}\,m^2$, longitudinal dispersivity is α_L = 3 mm. DOC reaction rate is $k_{DOC} = 5 \cdot 10^{-6}\ s^{-1}$, nitrification rate is $k_n = 5 \cdot 10^{-6}$ L/(**mg·s**). In-stream concentrations are shown in Table 2. Vectors are only indicative of flow direction.

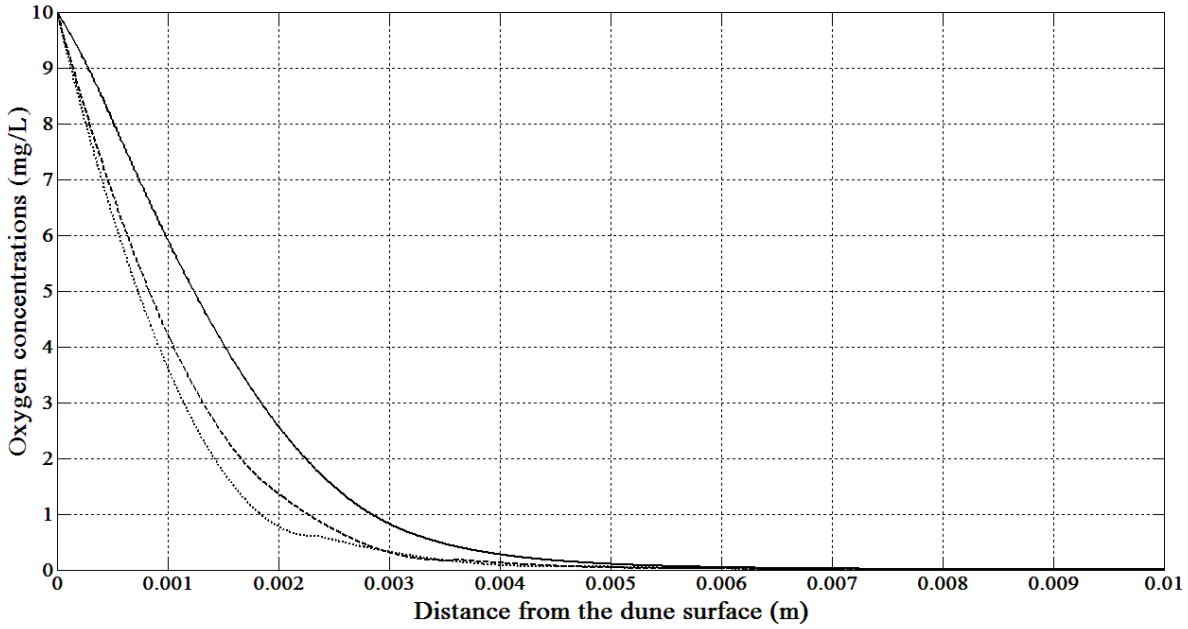

Fig. 6. Oxygen concentrations for case 2, under diffusive conditions, at x = 0 m (solid line), x = 0.5 m (dashed line) and x = 0.9 m (dotted line).

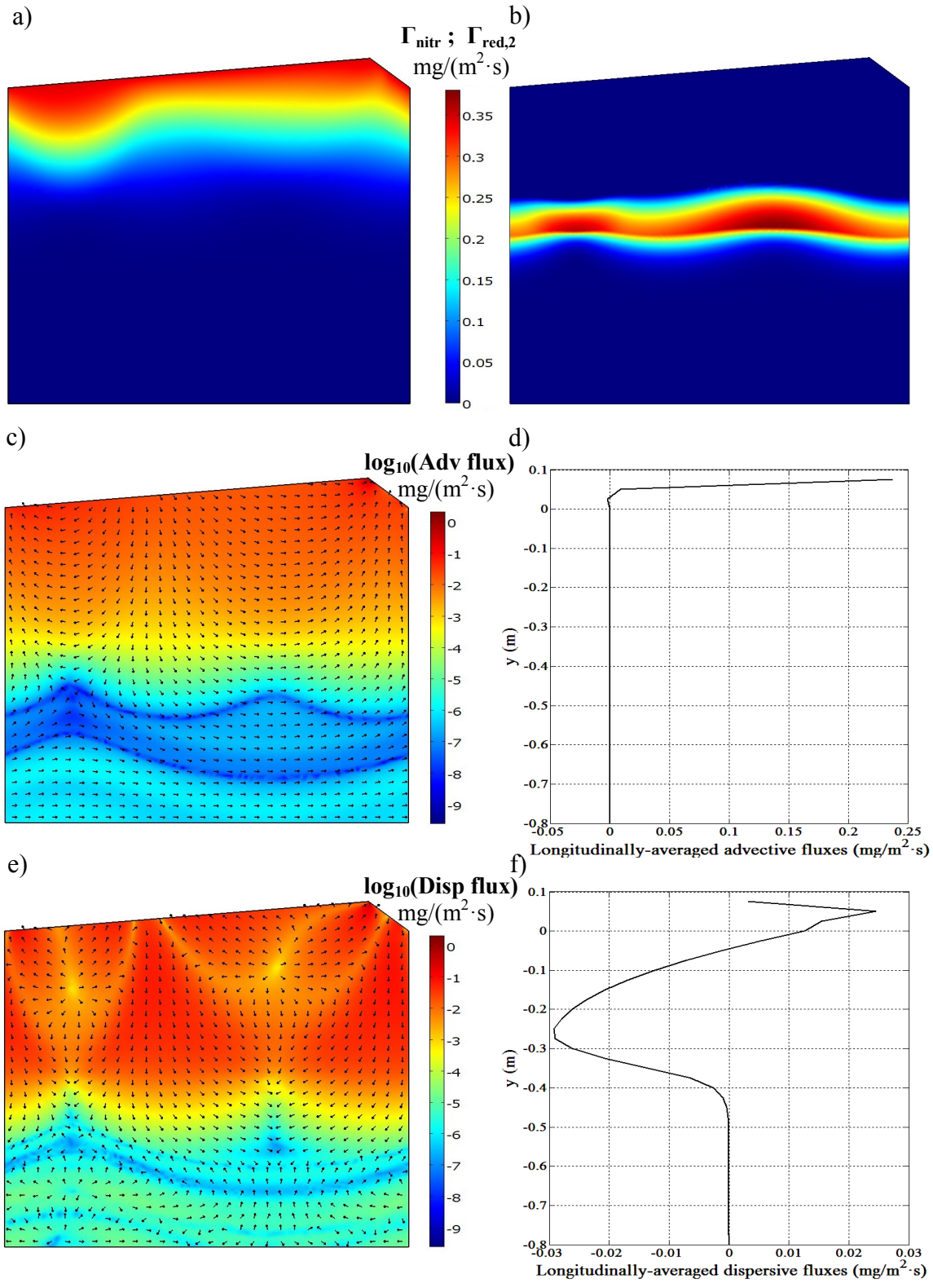

Fig. 7. Nitrification and denitrification rates (Fig. 7a, 7b), logarithmic values and longitudinally-averaged vertical profiles of advective (Fig. 7c, 7d) and dispersive (Fig. 7e, 7f) fluxes of nitrate (case 1). Vectors are only indicative of flux direction.

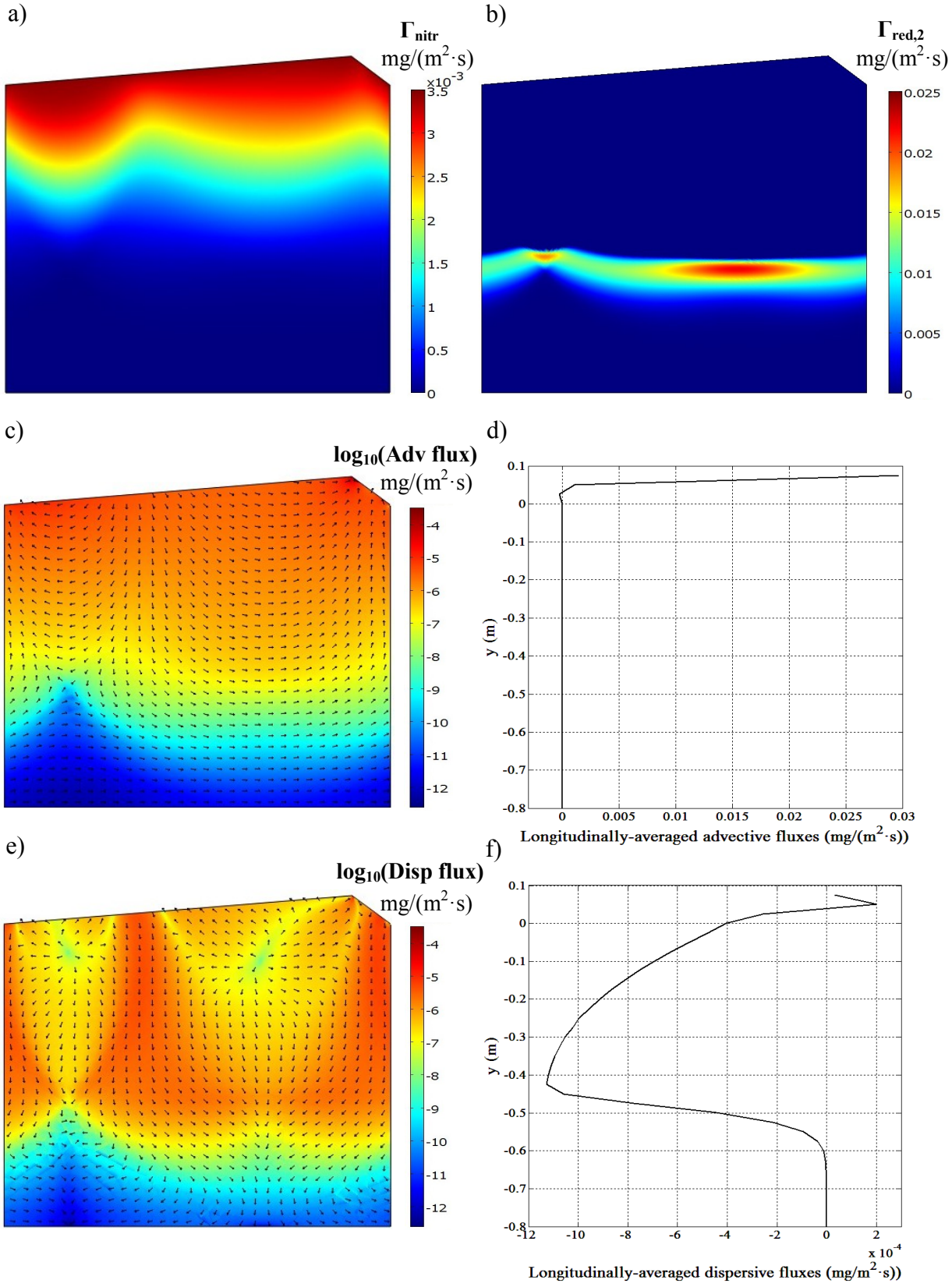

Fig. 8. Nitrification and denitrification rates (Fig. 8a, 8b), logarithmic values and longitudinally-averaged vertical profiles of advective (Fig. 8c, 8d) and dispersive (Fig. 8e, 8f) fluxes of nitrate (case 2). Vectors are only indicative of flux direction.

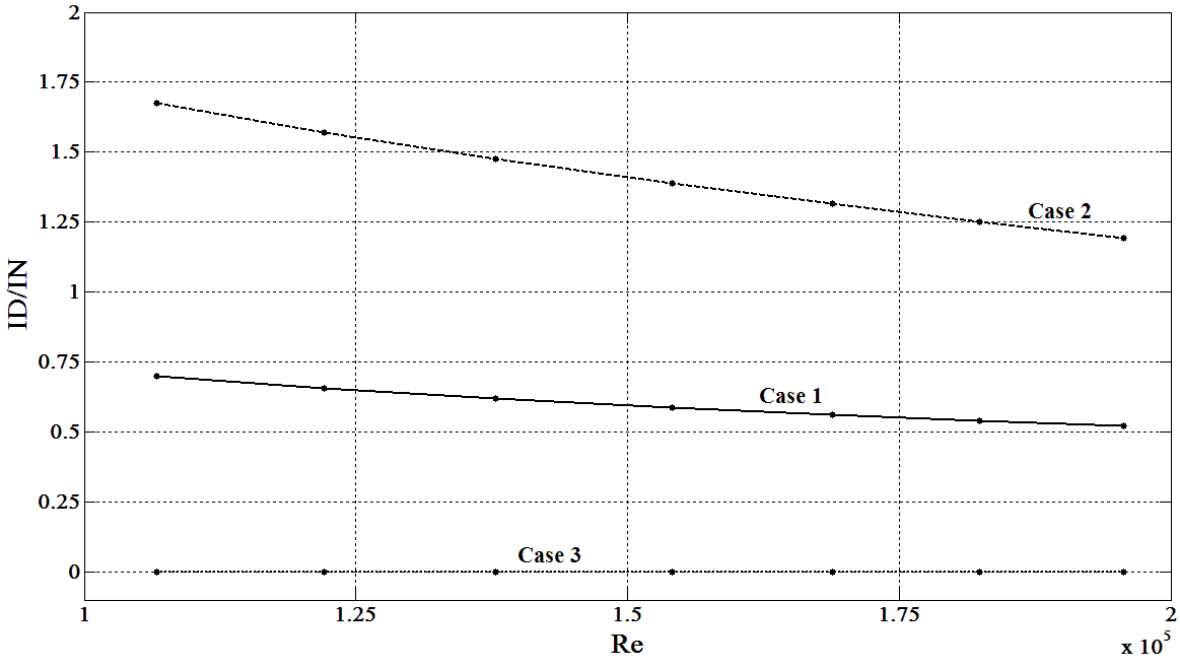

Fig. 9. Ratio of ID to IN rates vs. Reynolds numbers for case 1 (solid line), case 2 (dashed line) and case 3 (dotted line).

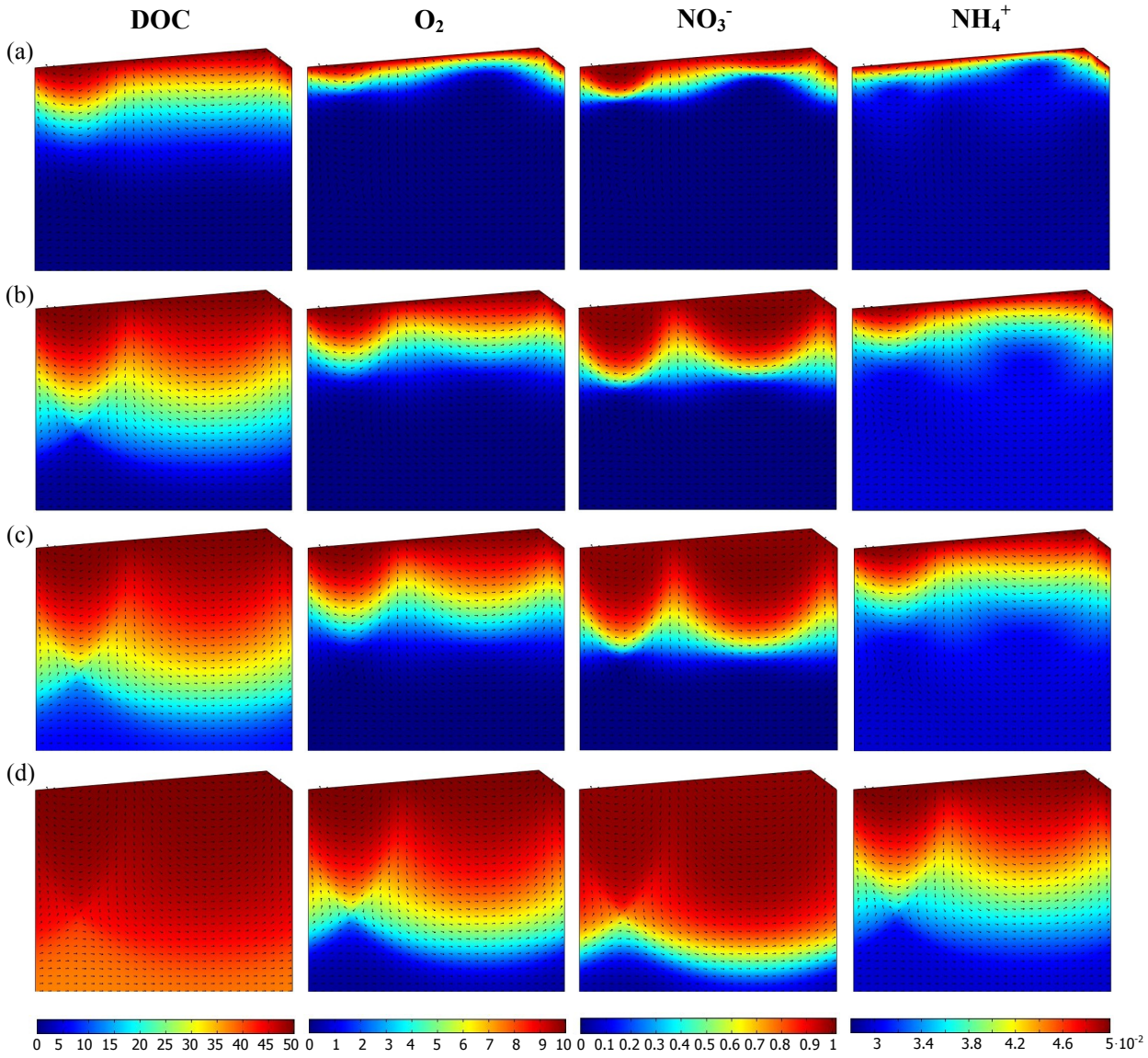

Fig. 10. Solute spatial distributions for case 2 (see Table 2), with stream velocity U = 0.27 m/s and sediment permeabilities $\kappa = 10^{-11}$ m^2 (Fig. 9a), $5\cdot10^{-11}$m^2 (Fig. 9b), 10^{-10} m^2 (Fig. 9c), $5\cdot10^{-10}$ m^2 (Fig. 9d). DOC reaction rate is $k_{DOC} = 5\cdot10^{-6}$ s^{-1}, nitrification rate is $k_n = 5\cdot10^{-6}$ L/(mg·s). All concentrations are expressed in mg/L.